Gas around galaxy haloes - III: hydrogen absorption signatures around galaxies and QSOs in the Sherwood simulation suite

Avery Meiksin[1⋆], James S. Bolton[2], Ewald Puchwein[3]
[1]*SUPA†, Institute for Astronomy, University of Edinburgh, Blackford Hill, Edinburgh EH9 3HJ, UK*
[2]*School of Physics and Astronomy, University of Nottingham, University Park, Nottingham NG7 2RD, UK*
[3]*Kavli Institute for Cosmology and Institute of Astronomy, Madingley Road, Cambridge, CB3 0HA, UK*

Accepted . Received ; in original form

ABSTRACT

Modern theories of galaxy formation predict that galaxies impact on their gaseous surroundings, playing the fundamental role of regulating the amount of gas converted into stars. While star-forming galaxies are believed to provide feedback through galactic winds, Quasi-Stellar Objects (QSOs) are believed instead to provide feedback through the heat generated by accretion onto a central supermassive black hole. A quantitative difference in the impact of feedback on the gaseous environments of star-forming galaxies and QSOs has not been established through direct observations. Using the Sherwood cosmological simulations, we demonstrate that measurements of neutral hydrogen in the vicinity of star-forming galaxies and QSOs during the era of peak galaxy formation show excess Lyman-α absorption extending up to comoving radii of ~ 150 kpc for star-forming galaxies and $300-700$ kpc for QSOs. Simulations including supernovae-driven winds account for the absorption around star-forming galaxies but not QSOs.

Key words: cosmology: large-scale structure of Universe – quasars: absorption lines – galaxies: formation – intergalactic medium

1 INTRODUCTION

The paradigm of cosmological structure formation through the growth of primordial density fluctuations predicts galaxies reside within accreting haloes at the interstices of a cosmic web of dark matter and gas. The most straightforward estimates of the expected stellar content of galaxies, however, suggest a conversion rate of infalling gas into stars that is too high. Galaxies should be much brighter than measured. It is widely believed some form of feedback must regulate the efficiency of star formation. Both semi-analytic models and cosmological hydrodynamics simulations suggest two forms of feedback are in play: stellar and supernovae-driven galactic winds in star-forming galaxies and heating generated through accretion onto a supermassive black hole in galaxies with an Active Galactic Nucleus (AGN) (see the review by Somerville & Davé 2015). The estimated galactic stellar mass dividing star-forming galaxies from the most massive AGN, Quasi-Stellar Objects (QSOs), corresponds to a dark matter halo mass of about $10^{12}\,\mathrm{M}_\odot$ (Kauffmann et al. 2003; Trainor & Steidel 2012). This is the halo mass for which the efficiency of gas conversion into stars peaks (Behroozi et al. 2013).

The opportunity to detect direct evidence for any difference in the environmental impact between star-forming galaxies and QSOs, however, has been wanting. This has now changed with the advent of observational programmes that probe the gaseous surroundings of galaxies and QSOs. Utilizing the large-scale QSO surveys from the Sloan Digital Sky Survey (York et al. 2000; Schneider et al. 2005) and its extension to the Baryon Oscillation Spectroscopic Survey (Croom et al. 2004), the Quasar-Probing-Quasar survey (QPQ) (Hennawi et al. 2006) has used lines of sight to 149 QSOs to probe the gaseous surroundings of both foreground QSOs (Prochaska & Hennawi 2009; Prochaska et al. 2013) and galaxies (Prochaska et al. 2013). Similarly, the Keck Baryonic Structure Survey (KBSS) (Rakic et al. 2012; Rudie et al. 2012; Trainor & Steidel 2012) has used lines of sight to 15 hyperluminous QSOs to measure gaseous absorption through the extended haloes of more than a thousand galaxies. Interest has particularly focussed on the central few hun-

⋆ E-mail: A.Meiksin@ed.ac.uk (AM)
† Scottish Universities Physics Alliance

dred kiloparsecs, the Circumgalactic Medium (CGM), since this is the arena in which supernovae-driven winds in star-forming galaxies and heating driven by black hole accretion in QSOs are expected to have their greatest impact (e.g. Kay et al. 2002; Schaye et al. 2010; van de Voort et al. 2011; Haas et al. 2013).

The QPQ and KBSS results demonstrate galaxies and QSOs are surrounded by excess amounts of Lyman-α absorption over that arising from the large-scale distribution of gas, the Intergalactic Medium (IGM) (Hennawi et al. 2006; Steidel et al. 2010; Rakic et al. 2012; Prochaska et al. 2013). Measuring the departures from the absorption predictions of models that exclude feedback provides a novel means of quantifying the impact of the winds and black hole accretion. Matching the excess absorption provides a test of feedback models. Accounting for the covering fractions of neutral hydrogen absorption systems, especially those optically thick to photoionizing radiation, has proven particularly challenging. Motivated by the search for evidence of cold streams feeding the growth of galaxies (Birnboim & Dekel 2003; Kereš et al. 2005), early simulations produced substantially smaller covering fractions in massive haloes than measured. More recent simulations have had greater success, but still have not fully accounted for the observations. Using the FIRE "zoom-in"simulations (Hopkins et al. 2014), which include feedback from stellar winds and supernovae but not from AGN, Faucher-Giguère et al. (2015) reproduced the average covering fraction of Lyman Limit Systems, absorbers optically thick at the Lyman edge ($N_{\rm HI} > 10^{17.2}\,{\rm cm}^{-2}$), for lines of sight passing within the virial radius of star-forming galaxies, as measured by Rudie et al. (2012), but not for the QSO measurements of Prochaska et al. (2013). The model prediction for star-forming galaxies for the average covering fraction within the virial radius of absorption systems with $N_{\rm HI} > 10^{15.5}\,{\rm cm}^{-2}$ was a factor ~ 2 short of measurements. On increasing the mass resolution, Faucher-Giguère et al. (2016) were able to reproduce the covering fraction of optically thick absorbers within the virial radius of QSOs. Notably AGN feedback was still not included. Using a different zoom-in simulation with feedback from stellar winds and supernovae, but not AGN (Dekel et al. 2013, and references therein), Fumagalli et al. (2014) found a covering fraction for optically thick absorbers within the virial radius of star-forming galaxies about half that measured, but consistent within the broad observational error. The prediction for QSOs fell well short of measurements. The dark matter particle mass was only twice that of the higher resolution FIRE simulations used, but the baryon mass resolution achieved may have been considerably poorer. The simulations also over-predict the stellar content of the galaxies by a factor of two, so that the gas content was likely too low. Using a suite of cosmological hydrodynamics simulations with a variety of wind feedback models, both with and without AGN feedback, Suresh et al. (2015) found some of the models match the cumulative covering fraction of optically thick absorbers within the virial radius of star-forming galaxies, but the predicted values are about half the measured value within twice the virial radius. In an analysis of the EAGLE simulations (Schaye et al. 2015), for which a different supernova-driven wind feedback model was implemented and which include AGN heating, Rahmati et al. (2015) matched the covering fraction profile of systems with column densities exceeding $10^{15.5}\,{\rm cm}^{-2}$ around star-forming galaxies for lines of sight with a range of impact parameters both inside and outside the virial radii. They were similarly able to reproduce the profiles for the covering fractions of optically thick systems around QSOs. As noted by Faucher-Giguère et al. (2016), however, the covering fraction of optically thick absorbers increases rapidly with halo mass and Rahmati et al. (2015) confined their comparison to QSO halo virial masses $M_h > 10^{12.5}\,{\rm M}_\odot$. Observations favour a somewhat lower mass range (Trainor & Steidel 2012; White et al. 2012; Eftekharzadeh et al. 2015). Since the simulation used included AGN feedback, it is also not known whether supernovae-driven winds would have been sufficient. The mass resolution of the simulation was moreover intermediate between the FIRE simulations that succeeded in reproducing the covering fraction around QSOs without AGN feedback and those that failed, so it is not known if this is a critical factor as well. On the other hand, an advantage of cosmological simulations over zoom-in simulations is the large sample size, with over a hundred QSO halo mass systems at $z = 2$ in the EAGLE simulation, which may be more representative of the population than the ~ 15 systems available in the FIRE simulation, and fewer in the Fumagalli et al. (2014) analysis.

The covering fractions do not provide a full description of hydrogen absorption around galaxies and QSOs. The collective absorption may be quantified additionally by the integrated equivalent width of absorption along the line of sight, or, analogously, the excess in the mean absorbed flux over the contribution from the diffuse IGM. Using a zoom-in simulation of a single galaxy including supernovae-driven wind feedback, Shen et al. (2013) matched the equivalent widths measured outside the virial radii of star-forming galaxies in the KBSS survey (Steidel et al. 2010; Rakic et al. 2012), but the predictions fell nearly a factor of two short for lines of sight with impact parameter at about half the virial radii, not much different from the case with no feedback (Meiksin et al. 2015). The simulations successfully reproduced the mean covering fraction of optically thick absorbers within the virial radii of star-forming galaxies, but were a factor of two low at twice the virial radius. The covering fraction for systems with $N_{\rm HI} > 10^{15.5}\,{\rm cm}^{-2}$ was also low compared with the measured values. The virial mass of the galaxy halo was $2.6 \times 10^{11}\,M_\odot$, somewhat low for the population of star-forming galaxies in the KBSS survey, but the results illustrate that a variety of absorption measurements, including profile information, must be used to demonstrate that a simulation model gives an accurate representation of the distribution of neutral hydrogen around galaxies.

A principal goal of this paper is to establish the scale of departure of the gaseous haloes around galaxies from the non-feedback cosmic-web prediction. Previously we found models without feedback matched the observed absorption signatures of the "mesogalactic medium" at distances exceeding $500 - 800$ comoving kpc around galaxies with halo masses up to $10^{12}\,{\rm M}_\odot$ at redshifts $2 < z < 2.5$ (Meiksin et al. 2015); the simulation volumes were too small to make firm statements for larger mass haloes. By contrast, clear excesses in the data compared with the non-feedback models were found within the inner $100-300$ comoving kpc (Meiksin et al. 2015). Using the Sherwood simulation suite (Bolton et al. 2016), we reinvestigate the signatures of hydrogen ab-

sorption around galaxies and QSOs. We include simulations both without and with feedback, using a different feedback model compared with previous simulations in the context of CGM measurements to further test the sensitivity of the absorption signatures to the feedback model. These new larger box simulations also substantially improve the precision of the predictions, particularly for the rare massive haloes exceeding 10^{12} $M_\odot$, enabling us to quantify the differences between the absorption signatures below and above this mass threshold.

This paper is organized as follows. In Sec. 2 we summarise the numerical simulations used in this work. The resulting H I absorption signatures are presented in Sec. 3. We summarize and discuss our conclusions in Sec. 4. Simulation convergence tests are presented in an Appendix. Unless stated otherwise, all results are for a flat ΛCDM universe with the cosmological parameters $\Omega_m = 0.308$, $\Omega_b h^2 = 0.0222$ and $h = H_0/100$ km s^{-1} Mpc^{-1} $= 0.678$, representing the present-day total mass density, baryon density and Hubble constant, respectively. The power spectrum has spectral index $n_s = 0.961$, and is normalized to $\sigma_8 = 0.829$, consistent with the Cosmic Microwave Background data from *Planck* (Planck Collaboration et al. 2014). All distances are comoving unless stated otherwise; 'cMpc'is used to designate comoving megaparsecs, and 'ckpc'to designate comoving kiloparsecs.

2 NUMERICAL SIMULATIONS

The numerical simulations are performed using a modified version of the parallel Tree-PM SPH code `P-GADGET-3`, an updated version of the publicly available code `GADGET-2` (last described by Springel 2005). Both simulations without and with galactic winds were performed. Because the computational demands for generating a galactic wind from first principles are well beyond current resources, all wind feedback models rely on a subgrid approximation scheme. Previously (Meiksin et al. 2015), we had used a star-formation and feedback model with a constant wind velocity for all haloes (Springel & Hernquist 2003). Such models, however, do not well reproduce the luminosity function of galaxies. The wind simulation used here is based on the star-formation and wind model of Puchwein & Springel (PS13; 2013). This scheme is built on a subgrid model that allows for star formation in a multiphase interstellar medium, with the feedback provided by stochastic kinetic energy injection by assigning to particles entering the wind near the centre of a galaxy a kick velocity that scales with the escape velocity from the halo. The mass loading factor, defined as the ratio of the mass flow in the wind to the star formation rate, is proportional to the inverse square of the escape velocity, thus using a constant amount of energy per unit mass of stars formed for driving the wind. This form has been found to recover the luminosity function and luminosity-metallicity relation of Local Group satellite galaxies (Okamoto et al. 2010). It also reproduces the stellar mass function of galaxies over redshifts $z < 2$, the observed gas to stellar mass ratios and specific star formation rates as a function of stellar mass (Puchwein & Springel 2013), and a variety of other galaxy properties over a wide range of redshifts (Vogelsberger et al. 2013). It receives additional support from x-ray measurements. The measured linear proportionality of the diffuse soft x-ray luminosity of galaxies with the star formation rate (Mineo et al. 2012), is matched in an energy-driven wind model for an asymptotic wind velocity that scales approximately as $\dot{M}_*^{1/6}$ (Meiksin 2016). For a star-formation rate scaling approximately like the stellar mass (e.g. Elbaz et al. 2007) and the ratio of stellar mass to halo mass scaling approximately as the halo mass for halo masses $10^{11} < M_h < 10^{12}\, M_\odot$ (e.g. Behroozi et al. 2013), the scaling required by the x-ray measurements corresponds at least approximately to a wind velocity scaling like the halo escape velocity. The mass-loading factor for the wind model in the simulations has typical values of $1-10$. This is consistent with the values found for the FIRE simulations (Muratov et al. 2015). By contrast, the mass loading factor was less than unity for the galaxy in Shen et al. (2013). Mass loading factors have not been published for the EAGLE simulations.

Other feedback mechanisms are considered in the literature of galaxy formation simulations. Murray et al. (2005) consider winds driven by momentum-deposition from radiation pressure or supernovae. Keller et al. (2014) use a superbubble feedback model for which mass loading includes a contribution from thermal evaporation. Another possibly important wind driver is cosmic-ray pressure (Ipavich 1975), which has recently been used in cosmological galaxy formation simulations (Salem et al. 2014; Pakmor et al. 2016).

The computational methods are described in detail in Bolton et al. (2016). The runs used in this paper are summarized in Table 1. Except for the wind simulation, the computations use the "quick Lyα"method (qLyα), for which all gas cooler than 10^5 K and with an overdensity exceeding 1000 is converted into collisionless "star"particles (without feedback). This is a computational trick used in IGM simulations to significantly speed up the computation (Viel et al. 2004), and is not meant to represent the stellar content of real galaxies. A detailed comparison with similar simulations using the finite-difference code `Enzo` (Bryan et al. 2014), with no gas removal or feedback implemented, shows that, while the quick Lyα approximation reduces the circumgalactic gas density within the virial radius of haloes compared with `Enzo`, the integrated absorption signatures are unaffected along baselines comparable to those used in measurements (Meiksin et al. 2015), even for lines of sight passing within the virial radius. This was shown to be because the integrated absorption signals over baselines exceeding $\sim 1000\,\mathrm{km\ s^{-1}}$ are dominated by gas outside the virial radius for non-feedback models even for impact parameters smaller than the virial radius. We accordingly use the quick Lyα simulations to model the absorption signatures in the absence of feedback.

To interpret the large-scale mesogalactic absorption signal through the extended galactic haloes outside the circumgalactic region, we also compute simple one-dimensional spherically symmetric collapse models. We use the combined gravitating shell model and hydrodynamics finite difference code described in Meiksin (1994), modified to allow for a cosmology with a cosmological constant. To recover the asymptotic mean profile at large distances from the centre, we use the mean profile derived by Bardeen et al. (1986) as the initial density profile. Since the gas is smooth, it is necessary to adopt a method to represent the density fluctuations underlying the Lyα forest, without which the important ef-

Table 1. Summary of the simulations performed in this work. The columns, from left to right, list the simulation name, the comoving box size, the dark matter particle mass, the baryon particle mass, the comoving gravitational softening length and the method of gas removal/ wind feedback.

Name	Box size $[h^{-1}$ cMpc]	M_{dm} $[h^{-1}$ $M_\odot]$	M_{gas} $[h^{-1}$ $M_\odot]$	l_{soft} $[h^{-1}$ ckpc]	gas removal/ wind
40-2048	40	5.37×10^5	9.97×10^4	0.78	qLyα
80-2048	80	4.30×10^6	7.97×10^5	1.56	qLyα
40-1024	40	4.30×10^6	7.97×10^5	1.56	qLyα
40-1024-ps13	40	4.30×10^6	7.97×10^5	1.56	PS13
20-512	20	4.30×10^6	7.97×10^5	1.56	qLyα

fects of line blanketing will not be recovered. We do so by implementing the lognormal density fluctuation scheme of Bi (1993) and Bi & Davidsen (1997) along projected one-dimensional lines of sight through the spherically symmetric gas distribution. Details are described in Chongchitnan & Meiksin (2014). To describe the fluctuations within a halo, the density field is normalized to the local mean density of the halo.

For both the full cosmological simulation and the spherically symmetric code, atomic radiative cooling from hydrogen and helium are included, along with photoionization heating. Metal-line cooling is not included. Metal-line cooling negligibly affects the large-scale IGM, but may play an important role within galactic haloes following the distribution of metals by supernovae feedback. The gas is photoionized by a metagalactic ultra-violet background. The mean Lyα absorbed flux level is set in order to match the measurements of Becker et al. (2013). Radiative transfer of continuum radiation is not included in the computations. Radiative transfer normally has little effect on the temperature of absorption systems optically thick to hydrogen and helium ionizing photons because their density is sufficiently high that thermal balance is achieved. It will, however, affect the amount of hydrogen absorption in optically thick systems. Because the large velocity shearing of absorption systems within the virial radius increases the equivalent widths of the systems (Meiksin et al. 2015), especially in the presence of a wind, it is important to include radiative transfer effects for predicting the amount of absorption within the virial radii of the haloes. Ideally, self-consistent radiative hydrodynamics should be implemented, but this is beyond the scope of this work. Instead we post-process the ionization fractions using the approximate treatment of Rahmati et al. (2013). The effect the radiative transfer correction has on the absorption signature is described in the Appendix. The full effect including radiative hydrodynamics is still a largely unexplored topic.

We extract spectra of the Lyα forest following the standard procedure, as summarized in Meiksin et al. (2015). A full Voigt profile is used throughout the analyses. To match the resolution of the observations, we smooth the resulting spectra with a Gaussian of FWHM 125 km s^{-1} for comparison with Prochaska et al. (2013) and FWHM 8 km s^{-1} for comparison with Rakic et al. (2012). We extract spectra for a range of impact parameters around haloes identified in the simulations using the friend-of-friends algorithm, as described in Bolton et al. (2016). We base our comparison primarily on the Lyman-α absorption equivalent width integrated across velocity windows. Previously we found this provided an adequate description of the effect of overdense structures near the haloes on the absorption statistics (Meiksin et al. 2015). For a halo at measured velocity $v_{\rm halo}$ along a line of sight to a background QSO, the equivalent width at the Lyman-α wavelength λ_α is computed as

$$w(b_\perp, \Delta v) = \frac{\lambda_\alpha}{c} \int_{v_{\rm halo}-\Delta v/2}^{v_{\rm halo}+\Delta v/2} dv \left[1 - e^{-\tau_\alpha(b_\perp, v)}\right], \qquad (1)$$

over a velocity window of width Δv centred on the position of the halo, displaced transversely by an amount $b_\perp$. The equivalent width is then used to define the fractional change δ_F in the transmitted flux compared with the mean intergalactic value for the corresponding velocity window (Prochaska et al. 2013)

$$\delta_F(b_\perp, \Delta v) = \frac{w(b_\perp, \Delta v) - w_{\rm IGM}}{\Delta\lambda - w_{\rm IGM}}. \qquad (2)$$

Here $\Delta\lambda = \lambda_\alpha \Delta v/c$ and $w_{\rm IGM} = \Delta\lambda[1 - \exp(-\tau_{\rm eff})]$, where $\tau_{\rm eff}$ is the Lyman-α effective optical depth of the IGM.

In the Appendix we present a suite of convergence tests of the cosmological simulations, varying the mass resolution and box size. In brief, we find that a comoving box size of $40h^{-1}$ Mpc on a side with a dark matter particle mass resolution $4.30 \times 10^6\, h^{-1}\, M_\odot$ (1024^3 particles) yields adequate convergence. Further convergence tests of the absorption signatures are described in Meiksin et al. (2015).

3 RESULTS

3.1 Deviation of Lyα absorption from the mean IGM

The left-hand panel of Fig. 1 shows the mean spherically averaged gas overdensity around haloes of mass 10^{12} $M_\odot$ at redshift $z = 2.4$. The profiles are constructed by spherically averaging the gas distribution around each halo in radial bins, and then averaging the resulting spherical profiles over the haloes in a narrow halo mass bin centred at $10^{12}\, M_\odot$. Results are shown for two simulations in a $40h^{-1}$ Mpc comoving box, one with a dark matter particle mass resolution of $4.30 \times 10^6\, h^{-1}\, M_\odot$ (40-1024) and the other with a resolution of $5.37 \times 10^5\, h^{-1}\, M_\odot$ (40-2048). The density profiles for the models agree well, and largely match the predictions of the spherical collapse model. Deviations from the BBKS linear theory profile become pronounced only within the inner 5 cMpc.

The absorption excess δ_F relative to the mean IGM, averaged over a spectral window of width $\Delta v = 2000$ km s^{-1},

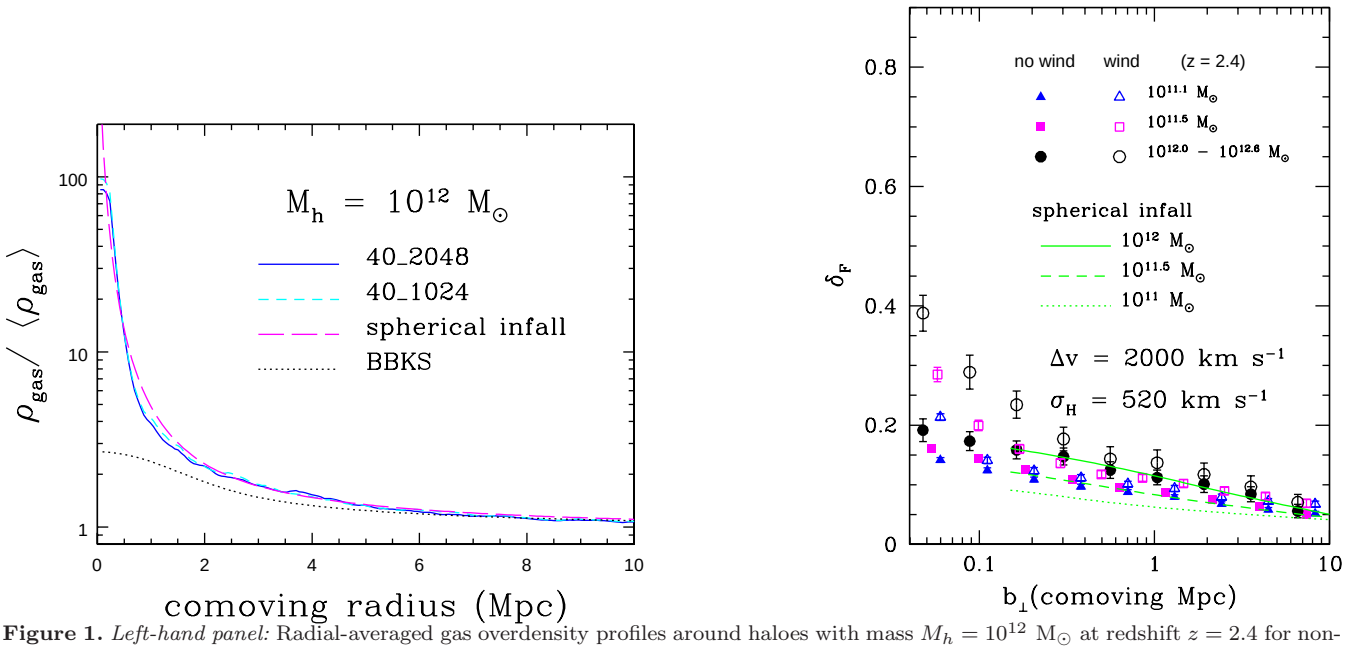

Figure 1. *Left-hand panel:* Radial-averaged gas overdensity profiles around haloes with mass $M_h = 10^{12}$ M$_\odot$ at redshift $z = 2.4$ for non-wind simulations with 2048^3 dark matter particles (40-2048; solid blue) and 1024^3 dark matter particles (40-1024; short-dashed cyan), both in a box $40h^{-1}$ comoving Mpc on a side. Also shown are the overdensity profiles for 1D spherical infall (long-dashed magenta) and the BBKS linear overdensity (dotted black). *Right-hand panel:* Fractional absorption excess δ_F relative to the mean IGM absorption, for a spectral window $\Delta v = 2000\,\mathrm{km\ s^{-1}}$ across the halo systemic velocities for the $40h^{-1}$ Mpc comoving box simulations with and without a wind, shown against projected impact parameter $b_\perp$ for halo masses $\log_{10}(M_h/M_\odot) = 11.1$ (triangles; blue), 11.5 (squares; magenta) and $12.0 - 12.6$ (circles; black) at redshift $z = 2.4$. For clarity of presentation, the points for the lowest and highest halo mass bins have been interpolated to slightly offset values of $b_\perp$. The halo velocities include a random component drawn from a Gaussian distribution with standard deviation $\sigma_\mathrm{H} = 520\,\mathrm{km\ s^{-1}}$. The curves (green) correspond to a 1D spherical infall model around haloes with masses $\log_{10}(M_h/M_\odot) = 11$, 11.5 and 12 (see text).

is shown in the right-hand panel of Fig. 1 for the non-wind simulation 40-1024 and the wind simulation 40-1024-ps13 at $z = 2.4$. A random line-of-sight halo velocity is allowed for, drawn from a Gaussian distribution with dispersion $\sigma_\mathrm{H} = 520\,\mathrm{km\ s^{-1}}$, typical of measurements (Prochaska et al. 2013). Results are shown as a function of projected line-of-sight comoving impact parameter $b_\perp$ for haloes in mass bins centred at $\log_{10}(M_h/M_\odot) = 11.1$ and 11.5 of width $\Delta \log_{10}(M_h/M_\odot) = 0.2$, and for haloes with masses $12.0 < \log_{10}(M_h/M_\odot) = 12.6$. The amount of absorption increases weakly with halo mass. While the wind simulation produces a greater amount of absorption for all impact parameters, δ_F is enhanced by the wind by an amount exceeding 0.05 only within the inner 50 ckpc for $\log_{10}(M_h/M_\odot) = 11.1$, 70 ckpc for $\log_{10}(M_h/M_\odot) = 11.5$ and 200 ckpc for $12.0 < \log_{10}(M_h/M_\odot) < 12.6$. For comparison, the corresponding virial radii are 160 ckpc, 220 ckpc and 320−510 ckpc, respectively, so that this level of enhancement occurs at about one-third the virial radii. As shown in the Appendix, when the impact parameters are rescaled to the virial radius for each halo mass, both the profiles without wind feedback and with are each nearly universal, independent of halo mass.

The spherically symmetric collapse models similarly predict an increase in δ_F with halo mass, as shown by the (green) curves in Fig. 1 (right-hand panel). The spherically symmetric solution is for an isolated halo. It neglects the average enhancement in absorption within the velocity window from the chance interception of other haloes clustered with the central halo. Estimating the correction analytically is not straightforward as it involves modelling the clustering of haloes in an overdense region. Instead we allow for a small additional amount of absorption common to all halo masses, normalizing to the absorption in the simulations at 7 cMpc. Allowing for the correction, the spherically symmetric model predictions agree closely with the non-wind numerical simulation from asymptotically large intergalactic scales to within the virial radii of the haloes.

3.2 Comparison with observations

We use the integrated absorption excess over broad velocity windows to quantify the absorption around galaxy haloes. Previously we found this provided an adequate description of the effect of overdense structures near the haloes on the absorption statistics (Meiksin et al. 2015).

In Fig. 2 we compare the predictions of models without and with winds to the δ_F measurements surrounding QSOs reported by Prochaska et al. (2013) at $z \approx 2.4$, with a velocity window $\Delta v = 2000\,\mathrm{km\ s^{-1}}$. A random component drawn from a Gaussian distribution with $\sigma_\mathrm{H} = 520\,\mathrm{km\ s^{-1}}$ is added to the halo velocities in the simulations to match the typical errors in the measured halo redshifts. The mean QSO halo mass at this epoch is $(1-3)\times10^{12}$ M$_\odot$ (Trainor &

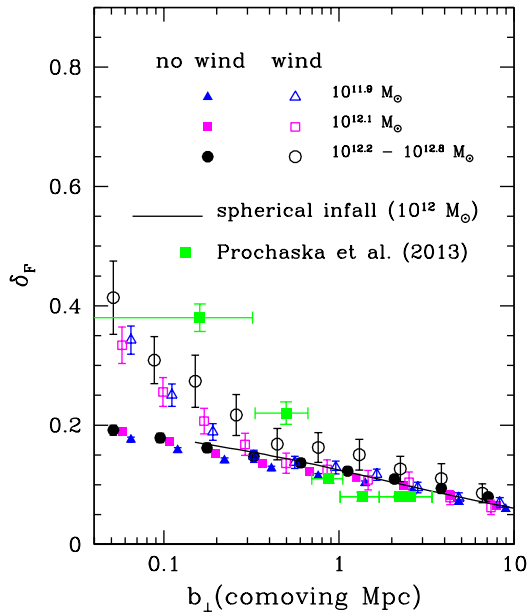

Figure 2. Absorption signature around QSOs. The fractional absorption excess δ_F relative to the mean IGM absorption is shown for a spectral window $\Delta v = 2000\,\mathrm{km\ s^{-1}}$ across the halo systemic velocities for the model without a wind (80-2048; solid symbols) and with a wind (40-1024-ps13; open symbols) at redshift $z = 2.4$, for halo masses $\log_{10}(M_h/M_\odot) = 11.9$ (triangles; blue), 12.1 (squares; magenta) and $12.2-12.8$ (circles; black). The solid line shows the prediction for simple spherical accretion. The data points (large green filled squares) are for absorption around QSOs at $z \approx 2.4$ taken from Prochaska et al. (2013), with the error bars showing the errors in the mean.

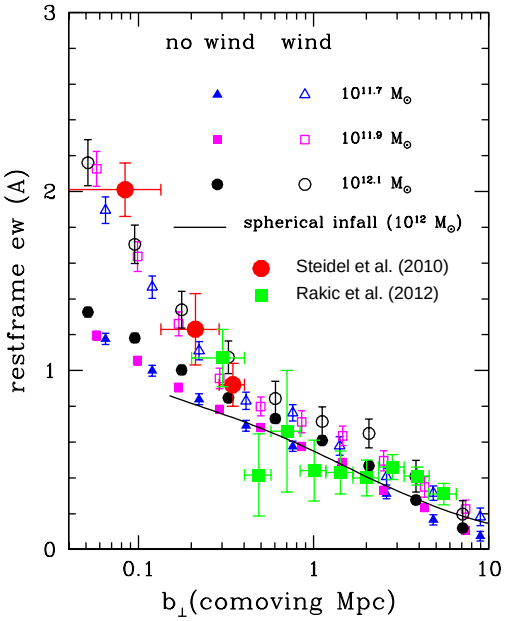

Figure 3. Absorption signature around star-forming galaxies. The rest-frame equivalent width (Å) is shown within a velocity window $\Delta v = 1000\,\mathrm{km\ s^{-1}}$ centred on the halo centre-of-mass velocity as a function of the line-of-sight impact parameter $b_\perp$ for halo masses $\log_{10}(M_h/M_\odot) = 11.7$ (triangles; blue), 11.9 (squares; magenta) and 12.1 (circles; black) at redshift $z = 2.4$ for models without wind feedback (80-2048; solid symbols) and with (40-1024-ps13; open symbols). The solid line shows the prediction for simple spherical accretion. The data are for star-forming galaxies from Steidel et al. (2010) (red filled circles) and Rakic et al. (2012) (large green filled squares).

Steidel 2012; White et al. 2012; Eftekharzadeh et al. 2015). Outside the virial radii (corresponding to $300-590$ comoving kpc for the halo masses shown), the measurements agree closely with the simulation predictions. The simulations slightly over-predict the amount of absorption near $1-2$ comoving Mpc. This may indicate too low a photoionization background was used, but we conservatively maintain the level used in the simulations. The measured values also match the expectation for spherical accretion onto a halo. The data show excess absorption over the non-wind model predictions at a statistically significant level (more than 3σ) out to impact parameters of $300-700$ comoving kpc, with the excess increasing with decreasing impact parameter. The wind model shows excess absorption over the non-wind model within the virial radii for the most massive haloes, but the amount still falls short of the measured values. The central two data points are more dominated by haloes with $z \simeq 2.0$ (Rahmati et al. 2015). The values for δ_F in the simulation at $z = 2.0$ agree within the errors with those at $z = 2.4$ or are somewhat smaller. The results suggest that while this particular wind model performs better than the constant velocity wind models studied previously (Meiksin et al. 2015), it is still not able to account fully for the high amounts of measured absorption. Alternatively, it may be an indication of the need to include AGN feedback.

In Fig. 3, we compare with the absorption equivalent widths measured around star-forming galaxies at $z \approx 2.4$ within $1000\,\mathrm{km\ s^{-1}}$ wide velocity windows centred on the systemic velocities of the galaxies using the data from Steidel et al. (2010) (red filled circles) and Rakic et al. (2012) (large green filled squares). A random component drawn from a Gaussian distribution with $\sigma_\mathrm{H} = 130\,\mathrm{km\ s^{-1}}$ is added to the halo velocities in the simulations to match the typical errors in the measured halo redshifts. A spatial correlation analysis gives an estimated median halo mass for the galaxies in the survey of $10^{11.9\pm0.1}\,\mathrm{M}_\odot$ (Trainor & Steidel 2012). We show results for halo mass bins centred at $\log_{10}(M_h/M_\odot) = 11.7$, 11.9 and 12.1 of width $\Delta\log_{10}(M_h/M_\odot) = 0.2$. Following the observational analysis procedure of Rakic et al. (2012) used to match their newer data to the continuum level of the earlier data of Steidel et al. (2010), the simulated spectra have been adjusted by applying a renormalization factor of 0.804 to the fluxes. Outside the virial radii ($250-350$ comoving kpc for the halo masses shown), the predicted equivalent widths of all the models agree well with the data within the measurement errors. They also agree with the prediction for spherical infall without feedback. Excess absorption over the non-wind model predictions is detected at a statistically significant level (more than 4σ) only within the inner $b_\perp < 140$ comoving kpc bin around the galaxies. The wind model now boosts the amount of absorption to match the measured levels. This contrasts with the constant velocity wind model,

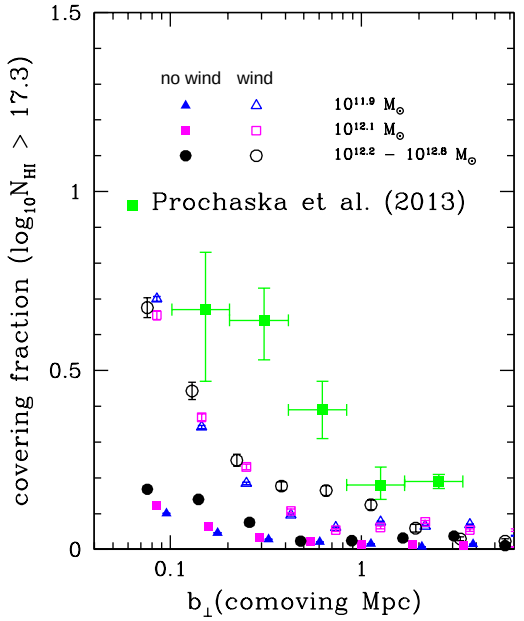

Figure 4. Covering fraction around QSOs. The covering fraction of H I gas with column density $\log_{10} N_{\rm HI} > 17.3$ is shown for a spectral window $\Delta v = 3000\,{\rm km\ s^{-1}}$ across the halo systemic velocities for the model without a wind (80-2048; solid symbols) and with a wind (40-1024-ps13; open symbols) at $z = 2.4$. The data points (large green filled squares) are from Prochaska et al. (2013) for absorption around QSOs at $z \sim 2.4$, with the error bars showing the errors in the mean.

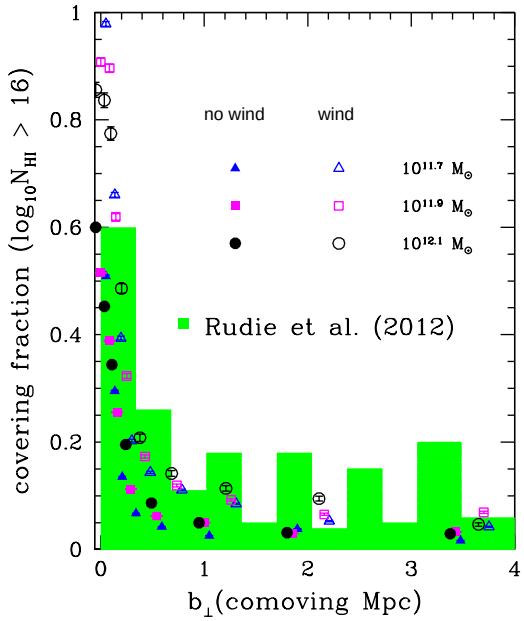

Figure 5. Covering fraction around star-forming galaxies. The covering fraction of H I gas with column density $\log_{10} N_{\rm HI} > 16.0$ is shown for a spectral window $\Delta v = 600\,{\rm km\ s^{-1}}$ across the halo systemic velocities for the model without a wind (80-2048; solid symbols) and with a wind (40-1024-ps13; open symbols) at $z = 2.4$. The data are from Rudie et al. (2012) for star-forming galaxies (green histogram).

for which too little absorption was found (Meiksin et al. 2015).

We have also checked against H I covering fractions around QSOs and star-forming galaxies. Fig. 4 shows the fraction of lines of sight through haloes with masses characteristic of QSOs that contain absorption systems with H I column densities exceeding $10^{17.3}\,{\rm cm^{-2}}$ at $z = 2.4$. The predicted covering fractions at $z = 2.0$ agree within the errors with those at $z = 2.4$ or are somewhat smaller. As we found previously (Meiksin et al. 2015), the covering fraction continues to fall short of the measurements of Prochaska et al. (2013), even for the new supernovae-driven wind model used here. Part of the discrepancy, such as near $1 - 2$ comoving Mpc, may be attributed to unresolved absorption systems (Prochaska et al. 2013), but not the steep rise towards small impact parameters. By contrast, Fig. 5 shows that the new wind model now recovers the H I covering fraction of systems around haloes with masses typical of star-forming galaxies, as measured by Rudie et al. (2012) for absorption H I column densities exceeding $10^{16}\,{\rm cm^{-2}}$. Rudie et al. (2012) also report cumulative covering fractions of 20 per cent. for systems with column densities in the range $10^{17.2} - 10^{20.3}\,{\rm cm^{-2}}$ for impact parameters within both the virial radius and twice the virial radius. We find 18 per cent. and 8 per cent., respectively. While the cumulative covering fraction within the virial radius is comparable to the measured value, the fraction within twice the virial radius is somewhat low.

4 DISCUSSION AND CONCLUSIONS

We use the Sherwood simulations, a suite of cosmological N-body+hydrodynamics IGM simulations, to predict absorption signatures around QSOs and star-forming galaxies. Both models without and with feedback in the form of supernovae-driven winds are included. No metals are included. In this paper, we use an energy-driven feedback model that scales the wind velocity with the escape velocity from the halo and varies the amount of mass loading as its inverse square, using a constant amount of mechanical energy per unit mass in stars formed to drive the wind. This contrasts with our previous treatment which invoked a wind with constant velocity and constant mass loading independent of halo mass.

A comoving box size of $40h^{-1}$Mpc with 1024^3 dark matter and gas particles each is shown to provide a well-converged estimate of the amount of absorption, when there are sufficient numbers of haloes. To produce accurate statistics for QSO haloes, however, a larger box size is preferred. We use a comoving box size of $80h^{-1}$Mpc with 2048^3 dark matter and gas particles each for comparison of the non-wind simulations with all observations. Because of the greater expense of the wind simulations, a $40h^{-1}$Mpc comoving box was used. An approximate analytic formulation is used to estimate the effects of radiative transfer on the absorption signatures in a post-processing step. For models without winds, the radiative transfer corrections negligibly affect the absorption signature, but the effects are non-negligible when a wind is included. The radiative transfer correction was ap-

plied in all cases for consistency. Radiative hydrodynamics effects are not taken into account.

Excellent agreement is found between the measured and predicted mesogalactic neutral hydrogen absorption signatures around star-forming galaxies outside the virial radius. Both line-of-sight absorption measurements and neutral hydrogen covering fractions are reproduced. This demonstrates that there is no need for the introduction of additional physical assumptions to describe the gas density and peculiar velocity fields for gas on these scales. Good agreement is also found well outside the virial radius for the QSO data. A small excess in the predicted amount of absorption may be a result of an under-estimated photoionizing radiation field. This may reflect an under-estimate of the metagalactic ionizing radiation background. It may also be an indication of a transverse proximity effect resulting from a local contribution to the ionizing radiation from the QSOs themselves, for which there is some independent evidence (Jakobsen et al. 2003; Syphers & Shull 2014). Outside the virial radius, the spherically averaged absorption signatures are still well described by spherical infall of intergalactic gas onto the haloes for both star-forming galaxies and QSOs, as predicted for the extended haloes of galaxies and QSOs forming at the peaks of a primordial gaussian field of density fluctuations, allowing for secondary infall.

By contrast, for impact parameters lying within the virial radii, statistically significant excess absorption is measured for both star-forming galaxies and QSOs compared with the non-feedback predictions. The excess absorption extends to substantially larger distances, of $300 - 700$ comoving kpc, around haloes exceeding $\log_{10}(M_h/M_\odot) = 12$, typical of those harbouring QSOs, than for the less massive haloes in which star-forming galaxies usually reside, for which excess absorption is measured only within the inner ~ 150 comoving kpc. This suggests that the affected region is larger around QSOs either because the feedback impact on the surrounding gas depends on halo mass beyond the scaling with virial radius found for the feedback model used, or because of a difference in the feedback mechanisms for star-forming galaxies and QSOs.

The supernovae-driven wind model used accounts for both the excess absorption around star-forming galaxies and the neutral hydrogen covering fraction, unlike our previous constant wind velocity simulations. The agreement suggests neither AGN heating nor metal cooling are required to match the absorption signatures for star-forming galaxies, although this conclusion may depend on the feedback model used. By contrast, even with the new feedback model, the simulations fail to account for the amounts of excess absorption and the covering fractions of optically thick gas near QSOs, even though the feedback model predicts the boost in absorption from the wind should increase with the halo mass at a fixed impact parameter. Additional heating by black-hole accretion may be required, although it may also indicate a need for higher numerical resolution of the gas.

ACKNOWLEDGMENTS

This work used the Curie supercomputer at the Tré Grand Centre de Calcul (TGCC) in France, made available through time awarded by the Partnership for Advanced Computing in Europe (PRACE) 8th Call. This work also made use of the DiRAC High Performance Computing System (HPCS) and the COSMOS shared memory service at the University of Cambridge. These are operated on behalf of the STFC DiRAC HPC facility. This equipment is funded by BIS National E-infrastructure capital grant ST/J005673/1 and STFC grants ST/H008586/1, ST/K00333X/1. We thank V. Springel for making `P-GADGET-3` available. JSB acknowledges the support of a Royal Society University Research Fellowship. EP acknowledges support by the Kavli Foundation.

REFERENCES

Bardeen J. M., Bond J. R., Kaiser N., Szalay A. S., 1986, ApJ, 304, 15
Becker G. D., Hewett P. C., Worseck G., Prochaska J. X., 2013, MNRAS, 430, 2067
Behroozi P. S., Wechsler R. H., Conroy C., 2013, ApJ, 770, 57
Bi H., 1993, ApJ, 405, 479
Bi H., Davidsen A. F., 1997, ApJ, 479, 523
Birnboim Y., Dekel A., 2003, MNRAS, 345, 349
Bolton J. S., Puchwein E., Sijacki D., Haehnelt M. G., Kim T.-S., Meiksin A., Regan J. A., Viel M., 2016, ArXiv e-prints, 1605.03462
Bryan G. L., Norman M. L., O'Shea B. W., Abel T., Wise J. H., Turk M. J., Reynolds D. R., Collins D. C., Wang P., Skillman S. W., Smith B., + 2014, ApJS, 211, 19
Chongchitnan S., Meiksin A., 2014, MNRAS, 437, 3639
Croom S. M., Smith R. J., Boyle B. J., Shanks T., Miller L., Outram P. J., Loaring N. S., 2004, MNRAS, 349, 1397
Dekel A., Zolotov A., Tweed D., Cacciato M., Ceverino D., Primack J. R., 2013, MNRAS, 435, 999
Eftekharzadeh S., Myers A. D., White M., Weinberg D. H., Schneider D. P., Shen Y., Font-Ribera A., Ross N. P., Paris I., Streblyanska A., 2015, MNRAS, 453, 2779
Elbaz D., Daddi E., Le Borgne D., Dickinson M., Alexander D. M., Chary R.-R., Starck J.-L., Brandt W. N., Kitzbichler M., MacDonald E., Nonino M., Popesso P., Stern D., Vanzella E., 2007, A&Ap, 468, 33
Faucher-Giguère C.-A., Feldmann R., Quataert E., Kereš D., Hopkins P. F., Murray N., 2016, MNRAS, 461, L32
Faucher-Giguère C.-A., Hopkins P. F., Kereš D., Muratov A. L., Quataert E., Murray N., 2015, MNRAS, 449, 987
Fumagalli M., Hennawi J. F., Prochaska J. X., Kasen D., Dekel A., Ceverino D., Primack J., 2014, ApJ, 780, 74
Haas M. R., Schaye J., Booth C. M., Dalla Vecchia C., Springel V., Theuns T., Wiersma R. P. C., 2013, MNRAS, 435, 2931
Hennawi J. F., Prochaska J. X., Burles S., Strauss M. A., Richards G. T., Schlegel D. J., Fan X., Schneider D. P., Zakamska N. L., Oguri M., Gunn J. E., Lupton R. H., Brinkmann J., 2006, ApJ, 651, 61
Hopkins P. F., Kereš D., Oñorbe J., Faucher-Giguère C.-A., Quataert E., Murray N., Bullock J. S., 2014, MNRAS, 445, 581
Ipavich F. M., 1975, ApJ, 196, 107
Jakobsen P., Jansen R. A., Wagner S., Reimers D., 2003, A&Ap, 397, 891

Kauffmann G., Heckman T. M., Tremonti C., Brinchmann J., Charlot S., White S. D. M., Ridgway S. E., Brinkmann J., Fukugita M., Hall P. B., Ivezić Ž., Richards G. T., Schneider D. P., 2003, MNRAS, 346, 1055
Kay S. T., Pearce F. R., Frenk C. S., Jenkins A., 2002, MNRAS, 330, 113
Keller B. W., Wadsley J., Benincasa S. M., Couchman H. M. P., 2014, MNRAS, 442, 3013
Kereš D., Katz N., Weinberg D. H., Davé R., 2005, MNRAS, 363, 2
Meiksin A., 1994, ApJ, 431, 109
Meiksin A., 2016, MNRAS, 461, 2762
Meiksin A., Bolton J. S., Tittley E. R., 2015, MNRAS, 453, 899
Mineo S., Gilfanov M., Sunyaev R., 2012, MNRAS, 426, 1870
Muratov A. L., Kereš D., Faucher-Giguère C.-A., Hopkins P. F., Quataert E., Murray N., 2015, MNRAS, 454, 2691
Murray N., Quataert E., Thompson T. A., 2005, ApJ, 618, 569, arXiv:astro-ph/0406070
Okamoto T., Frenk C. S., Jenkins A., Theuns T., 2010, MNRAS, 406, 208
Pakmor R., Pfrommer C., Simpson C. M., Springel V., 2016, ApJ, 824, L30
Planck Collaboration Ade P. A. R., Aghanim N., Armitage-Caplan C., Arnaud M., Ashdown M., Atrio-Barandela F., Aumont J., Baccigalupi C., Banday A. J., et al. 2014, A&Ap, 571, A16
Prochaska J. X., Hennawi J. F., 2009, ApJ, 690, 1558
Prochaska J. X., Hennawi J. F., Lee K.-G., Cantalupo S., Bovy J., Djorgovski S. G., Ellison S. L., Lau M. W., Martin C. L., Myers A., Rubin K. H. R., Simcoe R. A., 2013, ApJ, 776, 136
Prochaska J. X., Hennawi J. F., Simcoe R. A., 2013, ApJ, 762, L19
Puchwein E., Springel V., 2013, MNRAS, 428, 2966
Rahmati A., Pawlik A. H., Raicević M., Schaye J., 2013, MNRAS, 430, 2427
Rahmati A., Schaye J., Bower R. G., Crain R. A., Furlong M., Schaller M., Theuns T., 2015, MNRAS, 452, 2034
Rakic O., Schaye J., Steidel C. C., Rudie G. C., 2012, ApJ, 751, 94
Rudie G. C., Steidel C. C., Trainor R. F., Rakic O., Bogosavljević M., Pettini M., Reddy N., Shapley A. E., Erb D. K., Law D. R., 2012, ApJ, 750, 67
Salem M., Bryan G. L., Hummels C., 2014, ApJ, 797, L18
Schaye J., Crain R. A., Bower R. G., Furlong M., Schaller M., Theuns T., Dalla Vecchia C., Frenk C. S., McCarthy I. G., Helly J. C., Jenkins A., Rosas-Guevara Y. M., White S. D. M., 2015, MNRAS, 446, 521
Schaye J., Dalla Vecchia C., Booth C. M., Wiersma R. P. C., Theuns T., Haas M. R., Bertone S., Duffy A. R., McCarthy I. G., van de Voort F., 2010, MNRAS, 402, 1536
Schneider D. P., Hall P. B., Richards G. T., et al. 2005, AJ, 130, 367
Shen S., Madau P., Guedes J., Mayer L., Prochaska J. X., Wadsley J., 2013, ApJ, 765, 89
Somerville R. S., Davé R., 2015, ARA&A, 53, 51
Springel V., 2005, MNRAS, 364, 1105
Springel V., Hernquist L., 2003, MNRAS, 339, 289
Steidel C. C., Erb D. K., Shapley A. E., Pettini M., Reddy N., Bogosavljević M., Rudie G. C., Rakic O., 2010, ApJ, 717, 289
Suresh J., Bird S., Vogelsberger M., Genel S., Torrey P., Sijacki D., Springel V., Hernquist L., 2015, MNRAS, 448, 895
Syphers D., Shull J. M., 2014, ApJ, 784, 42
Trainor R. F., Steidel C. C., 2012, ApJ, 752, 39
van de Voort F., Schaye J., Booth C. M., Dalla Vecchia C., 2011, MNRAS, 415, 2782
Viel M., Haehnelt M. G., Springel V., 2004, MNRAS, 354, 684
Vogelsberger M., Genel S., Sijacki D., Torrey P., Springel V., Hernquist L., 2013, MNRAS, 436, 3031
White M., Myers A. D., Ross N. P., Schlegel D. J., Hennawi J. F., Shen Y., McGreer I., Strauss M. A., Bolton A. S., Bovy J., 2012, MNRAS, 424, 933
York D. G., Adelman J., Anderson Jr. J. E., et al. 2000, AJ, 120, 1579

APPENDIX A: CONVERGENCE TESTS ON H I STATISTICS

The convergence of the fractional absorption excess δ_F at $z = 2.4$ with mass resolution at a fixed comoving box size of $40\,h^{-1}$Mpc is tested in Fig. A1 for a velocity window of width $\Delta v = 1000\,\mathrm{km\ s^{-1}}$ and a halo redshift uncertainty $\sigma_\mathrm{H} = 130\,\mathrm{km\ s^{-1}}$, similar to the of observations of Rakic et al. (2012). A weak trend of increasing absorption with halo mass is found for decreasing impact parameters. For a given mass halo, there is no significant trend with particle mass, demonstrating the fluctuations in the gas giving rise to the absorption are well resolved. The absorption results shown in this paper use a mass resolution corresponding to a dark matter particle mass of $4.3 \times 10^6\,h^{-1}M_\odot$.

The convergence of the fractional absorption excess δ_F at $z = 2.4$ with comoving box size at a fixed mass resolution, corresponding to a dark matter particle mass $M_\mathrm{dm} \simeq 4.3 \times 10^6\,h^{-1}M_\odot$, is tested in Fig. A2. The same trend of increasing absorption with halo mass for decreasing impact parameter is recovered. For a given halo mass, there is no significant trend with simulation box size, although convergence is slowest at small impact parameters for the smallest halo mass bin. The results show that the large-scale power giving rise to fluctuations in the absorption has been well captured for the halo masses of interest. The absorption results in the paper are based on a simulation volume of comoving side $40\,h^{-1}$Mpc for models with a wind and $80\,h^{-1}$Mpc for models without.

We examine the possible role radiative transfer may play on the amount of absorption using the simplifying approximation of an attenuated radiation field within systems sufficiently dense to be self-shielded from an external photoionizing radiation field. We adopt the semi-analytic prescription of Rahmati et al. (2013), using a characteristic self-shielding total hydrogen density of $0.0064T_4^{0.17}\,\mathrm{cm^{-3}}$ for temperature $T_4 = T/10^4\,\mathrm{K}$. Fig. A3 shows the absorption excesses in a velocity window of width $\Delta v = 2000\,\mathrm{km\ s^{-1}}$, allowing for a halo redshift uncertainty $\sigma_\mathrm{H} = 520\,\mathrm{km\ s^{-1}}$, similar to the observations of Prochaska et al. (2013). For the non-wind models, we find the effect on the mean values of δ_F is under 5 per cent., and generally less than one

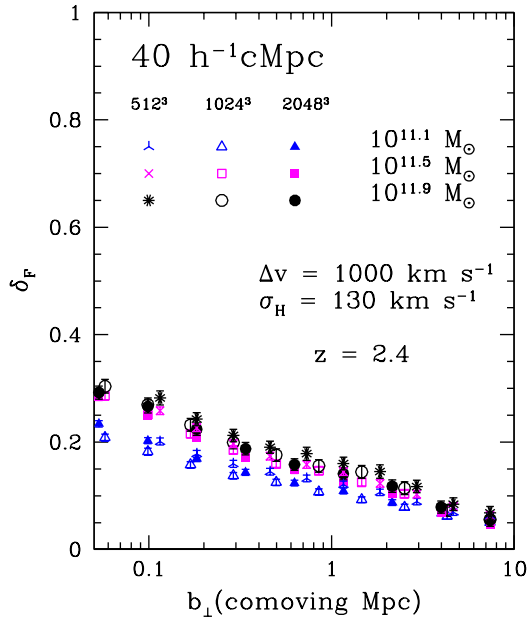

Figure A1. Fractional absorption excess δ_F relative to the mean IGM absorption for a velocity window $\Delta v = 1000\,\mathrm{km\ s^{-1}}$ around the halo centre-of-mass velocity. The data are shown as a function of the line-of-sight impact parameter $b_\perp$ for halo masses $\log_{10}(M_h/M_\odot) = 11.1$ (blue triangles), $\log_{10}(M_h/M_\odot) = 11.5$ (magenta squares) and $\log_{10}(M_h/M_\odot) = 11.9$ (black circles) at $z = 2.4$ for non-wind simulations in a comoving box size $40h^{-1}$ Mpc with dark matter particle mass resolutions of $3.44 \times 10^7\,h^{-1}\,\mathrm{M}_\odot$ (512^3 particles; starred symbols), $4.30 \times 10^6\,h^{-1}\,\mathrm{M}_\odot$ (1024^3 particles; open symbols), and $5.37 \times 10^5\,h^{-1}\,\mathrm{M}_\odot$ (2048^3 particles; filled symbols). No systematic differences with resolution are found within the errors, although the lowest resolution simulations show a small tendency towards slightly larger absorption deficits. Halo velocities include a random component drawn from a Gaussian distribution with standard deviation $\sigma_\mathrm{H} = 130\,\mathrm{km\ s^{-1}}$.

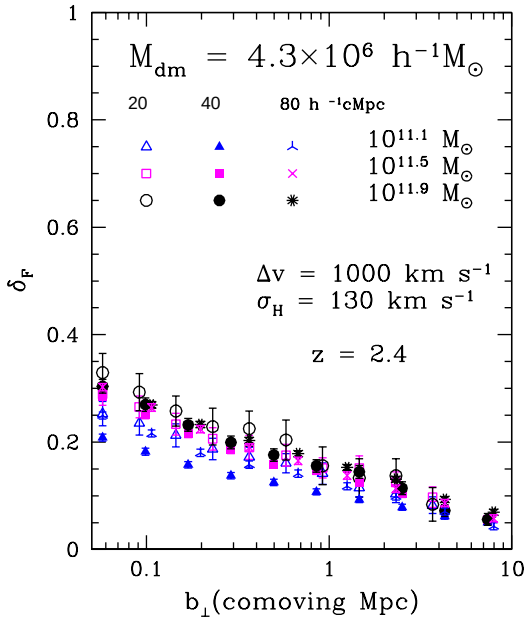

Figure A2. Fractional absorption excess δ_F relative to the mean IGM absorption within a $\Delta v = 1000\,\mathrm{km\ s^{-1}}$ window centred on the halo centre-of-mass velocity. The data are shown as a function of the line-of-sight impact parameter $b_\perp$ for halo masses $\log_{10}(M_h/M_\odot) = 11.1$ (blue triangles), 11.5 (magenta squares) and 11.9 (black circles) at redshift $z = 2.4$, for the non-wind simulations. No substantial differences are found between the box sizes within the errors, except for the smallest halo mass bin for which the convergence is somewhat slower. Halo velocities include a random component drawn from a Gaussian distribution with standard deviation $\sigma_\mathrm{H} = 130\,\mathrm{km\ s^{-1}}$.

per cent. By contrast, the wind simulation shows a marked increase in δ_F when the radiative transfer correction is included. The difference increases with increasing halo mass and decreasing impact parameter, reaching correction factors as high as 10–20 per cent. For consistency, in this paper we include the effects of radiative transfer for all the model predictions of the integrated amount of absorption.

For the wind model, which also creates stars following a more physically motivated model than the quick Lyman-α method does, we recomputed the halo centres and peculiar velocities by centring on the minimum of the gravitational potential rather than the centre-of-mass. The effects on the integrated absorption statistics and covering fractions were negligible, well within the dispersion in the mean values, except for a small boost in the H I covering fractions for the QSOs within the innermost 800 comoving kpc, but still within the statistical errors.

As shown in Fig. A4, rescaling the impact parameter to the virial radius of the halo masses in each halo mass bin results in nearly universal profiles for both the cases without and with wind feedback, independent of halo mass to within the Poisson errors. The enhancement in the amount of absorption produced by wind feedback is nearly independent of halo mass when expressed as a function of the rescaled impact parameters.

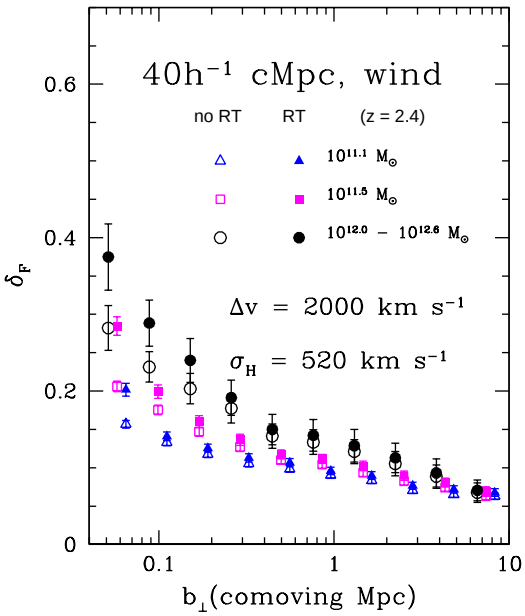

Figure A3. Fractional absorption excess δ_F relative to the mean IGM for halo masses $10^{11.1}\,M_\odot$ (blue triangles), $10^{11.5}\,M_\odot$ (magenta squares) and $12.0 < \log_{10}(M_h/M_\odot) < 12.6$ (black circles) within velocity windows of width $\Delta v = 2000\,\mathrm{km\ s^{-1}}$ in a $40h^{-1}$ Mpc comoving box for the simulation with galactic winds, at $z = 2.4$. The effects of corrections for radiative transfer are shown. The enhancement in absorption induced by the radiative transfer corrections increases with halo mass at a fixed impact parameter. Halo velocities include a random component drawn from a Gaussian distribution with standard deviation $\sigma_\mathrm{H} = 520\,\mathrm{km\ s^{-1}}$.

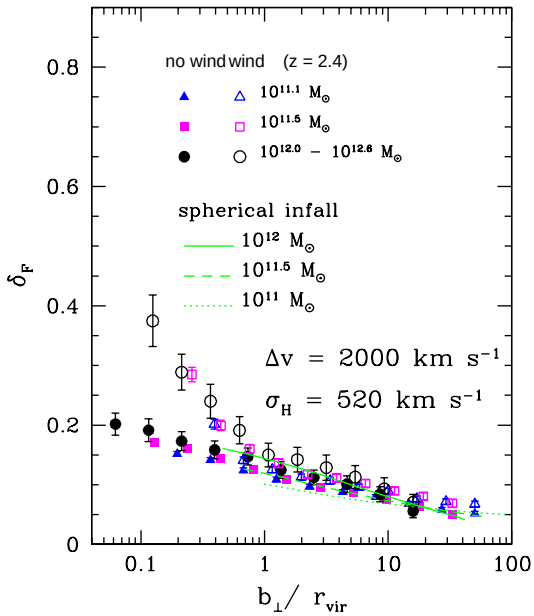

Figure A4. Fractional absorption excess δ_F relative to the mean IGM absorption, for a spectral window $\Delta v = 2000\,\mathrm{km\ s^{-1}}$ across the halo systemic velocities for the $40h^{-1}$ Mpc comoving box simulations with and without a wind, shown against projected impact parameter $b_\perp$, scaled to the virial radius r_vir, for halo masses $\log_{10}(M_h/M_\odot) = 11.1$ (triangles; blue), 11.5 (squares; magenta) and 12.0 – 12.6 (circles; black) at redshift $z = 2.4$. For clarity of presentation, the points for the lowest and highest halo mass bins have been interpolated to slightly offset values of $b_\perp/r_\mathrm{vir}$. The halo velocities include a random component drawn from a Gaussian distribution with standard deviation $\sigma_\mathrm{H} = 520\,\mathrm{km\ s^{-1}}$. The curves (green) correspond to a 1D spherical infall model around haloes with masses $\log_{10}(M_h/M_\odot) = 11$, 11.5 and 12.